ACS NANO
Cite This: ACS Nano 2018, 12, 12665−12672
www.acsnano.org

ARTICLE

Signatures of Topological Superconductivity in Bulk-Insulating Topological Insulator $BiSbTe_{1.25}Se_{1.75}$ in Proximity with Superconducting $NbSe_2$

Abhishek Banerjee, Ananthesh Sundaresh, Rajamanickam Ganesan, and P. S. Anil Kumar*

Department of Physics, Indian Institute of Science, Bengaluru 560012, India

Supporting Information

ABSTRACT: The combination of superconductivity and spin-momentum locking at the interface between an s-wave superconductor and a three-dimensional topological insulator (3D-TI) is predicted to generate exotic p-wave topological superconducting phases that can host Majorana Fermions. However, large bulk conductivities of previously investigated 3D-TI samples and Fermi level mismatches between 3D bulk superconductors and 2D topological surface states have thwarted significant progress. Here, we employ bulk-insulating topological insulators in proximity with two-dimensional superconductor $NbSe_2$ assembled *via* van der Waals epitaxy. Experimentally measured differential conductance yields unusual features including a double-gap spectrum, an intrinsic asymmetry that vanishes with small in-plane magnetic fields, and differential conductance ripples at biases significantly larger than the superconducting gap. We explain our results on the basis of proximity-induced superconductivity of topological surface states, while also considering possibilities of topologically trivial superconductivity arising from Rashba-type surface states. Our work demonstrates the possibility of obtaining p-wave superconductors by proximity effects on bulk-insulating TIs.

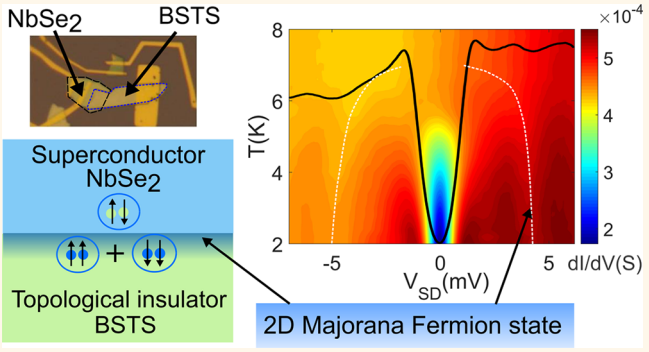

KEYWORDS: *topological superconductivity, Majorana Fermions, proximity effect, topological insulator, 2D superconductor, van der Waals heterostructure*

Proximity effects between topological insulators and superconductors have attracted significant attention as potential sources of unconventional superconductivity. Right after the discovery of three-dimensional topological insulators,[1−5] it became evident that inducing superconductivity into two-dimensional surface states of three-dimensional topological insulators (3D-TIs)[2,6−8] could lead to p-wave superconductivity,[9−12] where defects in the form of edges or vortices host Majorana Fermion states. In a different vein, it was also shown that inducing superconductivity into the "bulk" of topological insulators could lead to 3D topological superconductors whose surfaces could host surface Andreev bound states: essentially two-dimensional analogues of linearly dispersing Majorana Fermions.[13−17] Both these directions have been pursued vigorously with encouraging results, including purported demonstrations of surface Andreev bound states in $Cu_xBi_2Se_3$[13,14] and similar materials,[18] proximity effects on 3D-TI/superconductor interfaces,[19−26] Majorana zero modes in vortex cores of $Bi_2Te_3/NbSe_2$[27,28] heterostructure, and chiral 1D Majorana modes in Nb/quantum anomalous Hall insulator heterostructures.[29] Yet, a lot of these results remain ambiguous and can also be interpreted as consequences of more trivial effects. Experimental platforms that can manifest clear indications of topological superconductivity or Majorana Fermions in TIs are therefore highly sought after.

One of the primary sources of such ambiguity is the large bulk conductivity in first generation topological insulators like Bi_2Se_3. Most experiments on topological proximity effects have been performed on bulk conducting TIs,[19−28] and it is not clear whether the reported effects have topological origin. To remove these ambiguities it is imperative to induce superconductivity into topological surface states of *bulk-insulating* TIs, for instance, of the $Bi_xSb_{2-x}Te_ySe_{3-y}$ class. Such TIs achieve almost fully surface-state-dominated conduction and

Received: October 3, 2018
Accepted: November 26, 2018
Published: November 26, 2018

DOI: 10.1021/acsnano.8b07550
ACS Nano 2018, 12, 12665−12672

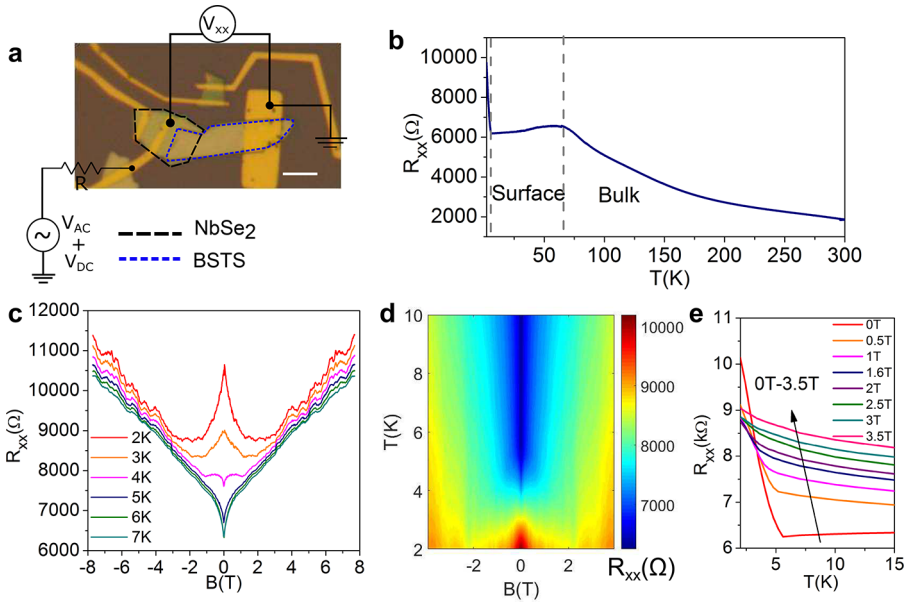

Figure 1. (a) Optical micrograph of a $NbSe_2$/$BiSbTe_{1.25}Se_{1.75}$ junction. Scale bar 5 μm. (b) Resistance *vs* temperature showing surface-dominated conduction. (c) Magnetoresistance measurements at different sample temperatures, (d) 2D color plot showing resistance as a function of magnetic field and temperature across the superconducting transition. (e) *R* vs *T* showing the superconducting transition at different magnetic fields

have sparked off a panoply of recent breakthroughs in condensed matter physics.[28,30−32] However, proximity effect between a superconductor and a bulk-insulating topological insulator remains difficult to achieve. Reduced bulk carrier densities and large Fermi surface mismatches between bulk three-dimensional superconductors like Nb and intrinsically two-dimensional topological surface states lead to weakly induced superconducting correlations. The inherent lack of surface bonding sites because of the layered nature of these materials may prevent strong chemical bonding with the superconductor, further exacerbating the problem. This may explain recent results on Nb/BSTS interfaces where electron−electron correlations rather than superconducting correlations appeared to dominate electrical transport.[33,34]

Several things must therefore conspire for topological superconductivity to occur in bulk-insulating TIs: (i) The host TI should be able to support large surface carrier density while maintaining negligible bulk carrier density. (ii) The chemical identities of the TI and SC must be similar to create a homogeneous interface that allows strong wave function overlap on either side. (iii) The Fermi surfaces on the SC and TI side should be well-matched to allow momentum conserved tunneling of quasiparticles. To this end, we fabricate van der Waals junctions between *bulk-insulating* topological insulator $BiSbTe_{1.25}Se_{1.75}$ (BSTS) and two-dimensional s-wave superconductor $NbSe_2$ and study their electrical transport properties. The chemical similarity between $NbSe_2$ and $BiSbTe_{1.25}Se_{1.75}$, the intrinsic two-dimensional Fermi surfaces of both materials and highly bulk-insulating nature of $BiSbTe_{1.25}Se_{1.75}$ all work in our favor. We unveil several signatures that are consistent with proximity induced superconductivity of the topological surface states including a differential conductance spectrum featuring two superconducting gaps, an intrinsic conductance asymmetry that vanishes when the induced superconductivity is quenched by an in-plane magnetic field and perhaps most strikingly, ripple-like features in the differential conductance spectra at biases considerably larger than the superconducting gap that vanish when bulk superconductivity is killed.

RESULTS AND DISCUSSION

Device Fabrication and Zero Bias Electrical Transport. $BiSbTe_{1.25}Se_{1.75}$ samples are obtained from the same crystal that has been used in our previous works to demonstrate large surface state transport, vanishing bulk conductivity, and quantum Hall effects.[35,36] $NbSe_2$ flakes are obtained from $NbSe_2$ single crystals with bulk T_c = 7.1 K. Heterostructures of $NbSe_2$/BSTS are prepared using an all-dry van der Waals transfer method. Subsequently, e-beam lithography followed by e-beam evaporation of Cr/Au 10 nm/100 nm is used to define electrical contacts to the sample. Details of device fabrication and single-crystal characterization can be found in Supporting Information sections A and B. Electrical transport experiments are performed using a low-frequency AC lock in method. The 10−20 nA AC bias currents are used throughout the experiments. For differential conductance measurements, the DC bias is generated using a 16-bit digital-to-analog converter and is added to the AC bias within a home-built setup. All measurements reported here use a current biased scheme.

Figure 1a depicts the optical micrograph of a typical device. Of the five total electrical contact lines, two contact the $NbSe_2$ layer and one large contact pad connects with the $BiSbTe_{1.25}Se_{1.75}$ layer. An extra pair of contact lines connect an adjoining $NbSe_2$ layer that is electrically isolated from the heterojunction device but can be used to calibrate the device temperature by measuring its superconducting transition. A large area of overlap is maintained between the BSTS and $NbSe_2$ layers. Resistance *versus* temperature ($R-T$) measurement (Figure 1b) at zero magnetic field shows characteristics of a typical bulk-insulating topological insulator. For T > 80 K, $R-T$ shows an insulating behavior originating from the gapped bulk states. The low-temperature range (5.6 K < T < 80 K) shows metallic transport arising from the topological surface

DOI: 10.1021/acsnano.8b07550
ACS Nano 2018, 12, 12665−12672

states. For T < 5.6 K, we observe a sharp nonsaturating increase in sample resistance, indicating an onset of superconductivity. The *rise* in resistance indicates that our samples are tuned into the so-called tunneling regime where Andreev reflection is suppressed due to the high bulk resistivity of our samples. This is essential to our experiments as the tunneling regime allows an accurate measurement of the density of states at the $NbSe_2$/TI interface.

Magnetoresistance measurements, depicted in Figure 1c, show a large zero-field resistance peak at T = 2 K. With an increase in magnetic field, the resistance peak is suppressed, showing negative magnetoresistance. This suppression continues until $B \sim 3.5$ T, after which positive magnetoresistance arising from weak antilocalization (WAL) of topological surface states takes over. With an increase in sample temperature, the negative MR peak gets suppressed, and a positive MR dip due to WAL becomes dominant and persists until very large temperatures ($T \simeq 30$ K). The suppression of the zero-field peak is clearly visible in the 2D resistance map shown in Figure 1d. Figure 1e shows a sequence of $R-T$ measurements at different magnetic fields. The zero-field measurement depicts a strong resistance upturn for T ≤ 5.6 K. Note that this temperature is lower than the transition temperature of bulk $NbSe_2$ (T_c = 7.1 K). At larger magnetic fields, the resistance upturn is suppressed, while the kink in $R-T$ curves (at T = 5.6 K at B = 0 T) shifts toward lower temperatures and becomes invisible at $B \simeq 3$ T. The field scale of B = 3 T roughly corresponds with the upper critical field H_{c2} = 3.5 T of $NbSe_2$.

Differential Conductance Measurements. To probe the presence of proximity effects, we perform two-terminal differential conductance measurements employing a two-probe measurement scheme in a current biased configuration as depicted in Figure 1a. The DC current biased differential conductance data are converted to the DC voltage biased differential conductance data, by taking into account the resistance of the unproximitized BSTS layer *not* contacted by $NbSe_2$, which appears in series with the BSTS/$NbSe_2$ junction resistance. The large resistivity of our bulk-insulating samples (3−7 kΩ/sq) makes this lead resistance an important parameter that must be accurately estimated. Note that using a four-probe geometry cannot alleviate this problem as such a configuration would only remove the Au-BSTS and Au-$NbSe_2$ contact resistances (∼200−500 Ω), which are much smaller than the lead resistance provided by the unproximitized BSTS layer. We therefore resort to Blonder−Tinkham−Klapwijk (BTK) theory[37] using the total lead resistance as a parameter to fit our experimental differential conductance data. We relegate the details of BTK fitting to Supporting Information section C. This produces a lead resistance of $R_l \simeq 4$ kΩ and the superconducting gap $2\Delta V_A \simeq 2.4$ mV, which agrees well with the superconducting gap of bulk $NbSe_2$, $2\Delta_0 \simeq 2.2$ mV. The DC voltage biased differential conductance data are obtained from the DC current biased differential conductance data (provided in Supporting Information section I) by subtracting the voltage drop across the contact resistance R_l and also removing the contribution of R_l to the measured differential conductance. We note that an error in estimation of the lead resistance R_l could, in principle, lead to an apparent shift in both the bias voltage and amplitude of various differential conductance features, resulting in possibly erroneous conclusions. However, our BTK fitting procedure determines the amplitude and temperature dependence of the superconducting gap Δ_0 of bulk $NbSe_2$ with a high degree of accuracy (see Supporting Information Figure S3k), indicating reasonable internal self-consistency. Furthermore, the saturation of $BiSbTe_{1.25}Se_{1.75}$ resistivity at low temperatures (T < 20 K) as observed clearly in the nonsuperconducting region of the R *versus* T data depicted in Figure 1b,e and in our previous works,[35] indicates that the lead resistance does not vary significantly in the temperature range of our interest (2−7 K), thereby minimizing the possibility of error in the estimation of R_l. Nonetheless, as the estimation of R_l is a subtle issue, to aid the reader, we have provided the raw differential conductance data as a function of the DC voltage bias, without correcting for R_l in Supporting Information section I.

The differential conductance data provide striking signatures of superconducting proximity effect as depicted in the 2D color plot of Figure 2a, where a strong zero bias conductance dip and

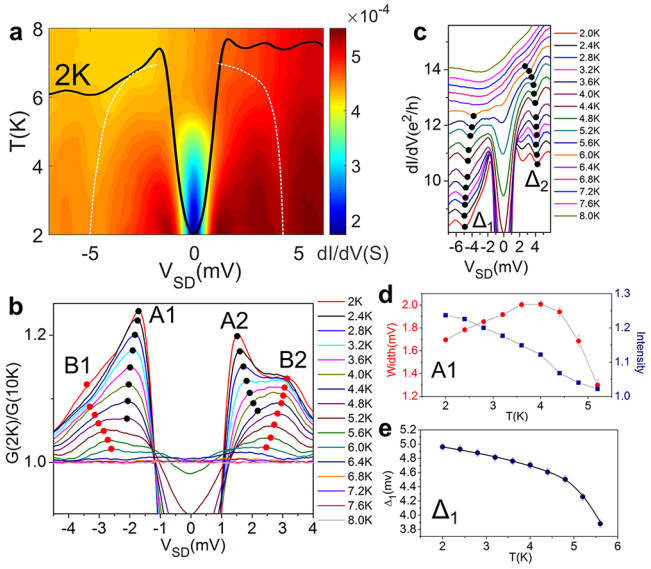

Figure 2. (a) 2D color plot of differential conductance as a function of temperature and source−drain DC voltage bias V_{SD}. (b) Normalized differential conductance $G(2\text{ K})/G(10\text{ K})$ showing a two-gap structure. The black and red dots track the evolution of coherence-like peak A1 (A2) and B1 (B2), respectively. (c) Differential conductance ripples Δ_1 and Δ_2 that exist at biases larger than the superconducting gap. Black dots trace their evolution with increasing temperature. (d) Evolution of the width and intensity of peak A1 with increasing temperature. (e) Evolution of position of the conductance dip at Δ_1 with increasing temperature.

series of peak/dip features at finite biases are observed. To rule out nonsuperconducting features, we follow the standard practice of normalizing the differential conductance data with the spectra obtained at T = 10 K just above the superconducting transition temperature of $NbSe_2$, as depicted in Figure 2b. We draw attention to several important features in the differential conductance spectra, before discussing each of these aspects in detail.

(i) First, the strong differential conductance dip at zero bias flanked by two sets of peaks (A1, A2 and B1, B2) indicative of two superconducting gaps. Such double-gap features have been observed previously in several proximity effect studies.[23,24] While the larger gap (B1 and B2) corresponds to electron tunneling into the unproximitized part of the superconductor away from the TI/SC interface, the smaller gap is usually

DOI: 10.1021/acsnano.8b07550
ACS Nano 2018, 12, 12665−12672

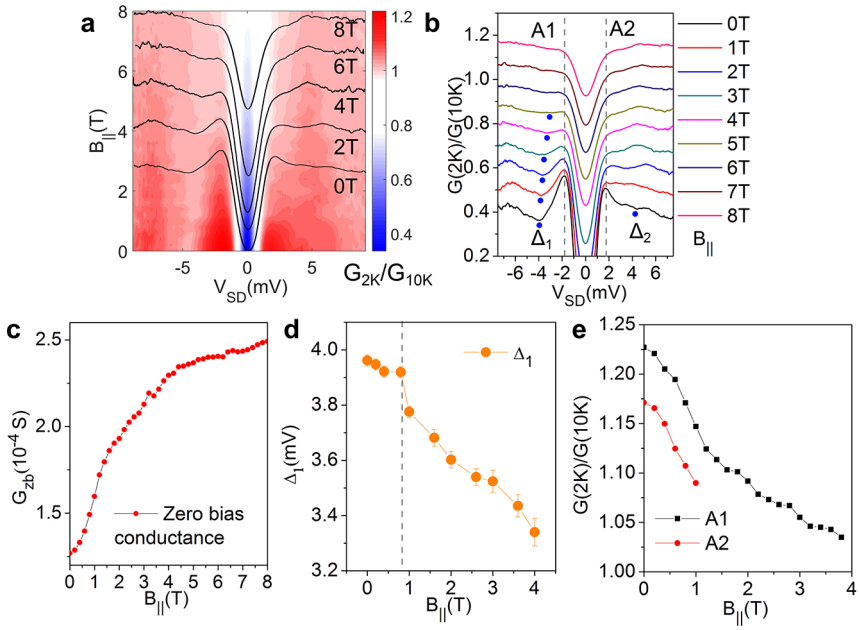

Figure 3. (a) 2D color plot of normalized differential conductance $G(2\text{ K})/G(10\text{ K})$ *vs* V_{SD} as a function of in-plane magnetic field. (b) Evolution of $G(2\text{ K})/G(10\text{ K})$ showing the breakdown of asymmetry with increasing in-plane magnetic field. The supergap ripples at Δ_1 and Δ_2 marked as blue dots also disappear. (c) Zero bias conductance G_{zb} as a function of in-plane magnetic field. (d) Evolution of bias position of dip at Δ_1 with $B_{\parallel}$. (e) Evolution of normalized coherence peak intensity at A1 and A2 with $B_{\parallel}$.

attributed to the inverse proximity effect, wherein the region of the SC in contact with the TI has reduced superconducting correlations. Equivalently, this gap can also be associated with electron tunneling into the topological surface state, which has now acquired a superconducting gap *via* the proximity effect. With increasing sample temperature, the peak positions of A1(A2) and B1(B2) show opposite behavior. While the gap at B1(B2) decreases, the gap at A1(A2) expands as plotted in Figure 2d, while the intensities of both peaks reduce. In fact, for $T \simeq 4.8$ K, A1(A2) completely vanishes and appears to merge with B1(B2). This further supports the proximity-induced origin of A1, in that it disappears well before B1 that corresponds to the parent superconductor.

(ii) Second, the dI−dV measurements show an intrinsic conductance asymmetry with respect to the sign of the DC bias voltage. The normalized conductance peak at A1 is considerably larger than its positive bias counterpart at A2. However, this asymmetry is less evident for peaks B1 and B2. In fact, the asymmetry disappears with increasing temperature and is roughly coincident with the merger of peaks A1(A2) and B1(B2). For $T \geq 4.4$ K, the asymmetry is completely absent.

(iii) Third, we observe several differential conductance ripples comprising consecutive dips and peaks at biases larger than the gap voltages. First, to ascertain whether these features have a superconducting origin or not, we analyze the temperature dependencies of the position of a pair of these dips with the strongest signature: Δ_1 and its positive bias counterpart Δ_2 appearing at $V_{SD} \simeq \pm 4-5$ meV. These appear as the striking dip-like features marked as white dashed lines in for Figure 2a and shown as Δ_1 and Δ_2 in Figure 2c. With increasing temperature, the dip feature collapses (Figure 2e) and completely disappears at $T \simeq 6$ K, indicating its superconducting origin. Such ripples have been previously reported in superconductors showing multiphonon effects like Pb[38] and correlated superconductors with magnonic excitations.[39] However, since the parent superconductor $NbSe_2$ shows no such effects, we can rule out such explanations because superconductivity in our samples is proximity induced. We point out that similar supergap features were recently observed in junctions of $NbSe_2$ and bulk conducting Bi_2Se_3.[25] However, the authors did not focus on this effect and provided no explanations for its origin.

Differential Conductance under In-Plane Magnetic Fields. We now explore how these features evolve upon the application of magnetic fields oriented parallel to the plane of the sample. As depicted in Figure 3a, the superconducting gap persists up to 8 T, the largest magnetic field attainable in our system. However, an examination of the normalized differential conductance G_{2K}/G_{10K} reveals that asymmetry between peaks A1 and A2 that is observed at low magnetic fields is completely extinguished for $B_{\parallel} \simeq 5$ T. In fact, notice how the entire dI−dV spectra that is highly asymmetric at $B_{\parallel} = 0$ T becomes highly symmetric at $B_{\parallel} = 8$T. Additionally, the supergap ripples, indicated as Δ_1 and Δ_2 in Figure 3b, also vanish with in-plane magnetic field and are completely suppressed at 5 T, as shown in Figure 3d for Δ_1. A critical value of $B_{\parallel} \simeq 5$ T also appears in the evolution of the zero bias conductance (G_{zb}) plotted in Figure 3c. With increasing magnetic field, G_{zb} rises sharply until around 5 T and then almost saturates.

We interpret this evolution as arising from two different superconducting orders: the low-field differential conductance corresponds to a combination of tunneling into the proximity induced topological surface state and the bulk superconductor $NbSe_2$. In general, increasing in-plane magnetic fields causes depairing of Cooper pairs due to orbital motion, thereby suppressing superconductivity. However, this effect is presumably stronger for the proximitized topological surface states, compared to two-dimensional $NbSe_2$, where it is known that Ising pairing between Cooper pairs causes superconductivity to survive at in-plane fields much larger than that dictated by the Pauli susceptibility limit.[40] Therefore, while proximity-induced

DOI: 10.1021/acsnano.8b07550
ACS Nano 2018, 12, 12665−12672

superconductivity and its consequent features including differential conductance asymmetry and supergap ripples are suppressed completely by $B_{||}$ = 5 T, the superconductivity in the Ising paired $NbSe_2$ survives and produces a symmetric differential conductance spectrum as expected for an s-wave superconductor.

The asymmetry in dI−dV therefore appears to be associated with the proximity-induced superconducting order, rather than superconductivity of bulk $NbSe_2$. The asymmetric spectrum has a natural explanation as a consequence of the linear density of states of the Dirac spectrum of topological surface states $D(E) \propto E$. When a superconducting gap is induced into the two-dimensional TSS, it retains its linear shape as the in-gap spectra must continuously match with the normal state spectra outside the gap. This is in contrast to bulk-derived 2D Rashba-type surface states that have finite mass and feature a constant density of states. The coherence peaks (A1 and A2) arising from the proximitisation of the TSS therefore retain an intrinsic asymmetry that vanishes when the sample temperature or magnetic field becomes large enough to close the TSS gap. Beyond such a temperature or magnetic field, only symmetric features originating from $NbSe_2$ are visible.

Differential Conductance under Perpendicular Magnetic Fields. Now we investigate differential conductance measurements in the presence of perpendicular magnetic fields,as shown in Figure 4a. We observe that superconductivity is suppressed at $B \simeq 3.5$ T, detected as a change in the variation of the zero bias conductance dip with magnetic field,as seen in Figure 4a (see also Figure 1c). For $0 < B \simeq 3.5$ T, zero bias conductance is enhanced, indicating destruction of superconducting order. Beyond this field, zero bias conductance gets suppressed as the sample enters into a regime where transport is dominated by a competition between a negative correction to conductance arising from electron−electron (e−e) interactions and a positive correction arising from WAL. The WAL effect is verified independently using magnetoresistance measurements presented in Figure 1c,d. In topological insulators, these two corrections almost cancel each other out in zero magnetic field. In a finite magnetic field, the positive correction due to WAL is suppressed due to broken time-reversal symmetry, thereby unmasking the negative conductance correction from e−e interactions. The applied voltage bias acts like an effective temperature that weakens the negative correction from e−e interactions, thereby leading to positive differential conductance as seen in Figure 4a for $B >$ 3.5 T. With increasing magnetic field, the zero bias conductance decreases as corrections from e−e interactions become more and more dominant. This distinction between superconductivity induced and e−e interaction induced differential conductance spectra is notable, particularly because previous experiments on superconducting proximity effects on bulk-insulating TIs have been mired by strong differential conductance signals arising from e−e interactions rather than superconducting correlations.[33,34]

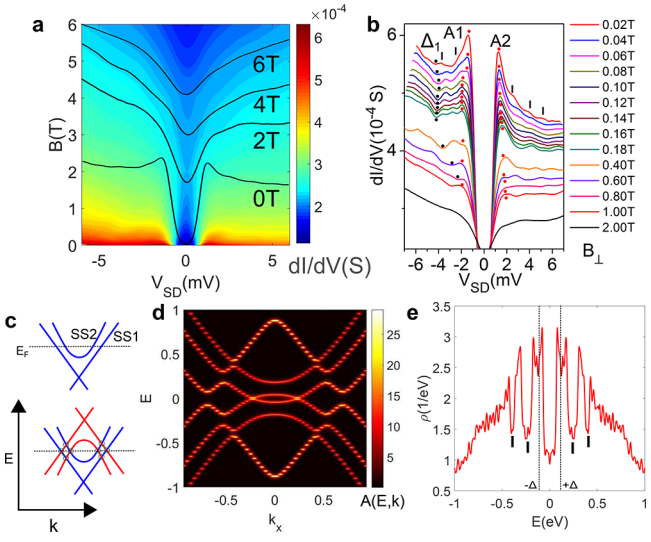

Figure 4. (a) 2D color plot of differential conductance as a function of out-of-plane magnetic field from 0 to 8 T. (b) Low field (0−2 T) evolution of differential conductance spectrum showing several ripples at supergap biases marked by vertical solid lines. (c) (Top) E−k band diagram of two surface confined states (SS1 and SS2) closely spaced in energy. (Bottom) Electron−hole excitation spectrum (no superconducting gap) showing band-crossings at the Fermi level and also at higher energies, indicative of interband Cooper pairing. (d) Spectral function evaluated for a multiband topological superconductivity in a thin slab of a TI. (e) Corresponding density of states showing mini-gaps at biases larger than the superconducting gap.

We now discuss the low-field measurements presented in Figure 4b. Specifically, we notice several differential conductance ripples above the superconducting gap that persist and even appear to get enhanced with small magnetic fields $B <$ 0.2 T. For larger fields, the ripples become nonuniform and completely disappear before reaching $B \simeq 2$ T. As we discussed before, these ripples cannot be explained as a consequence of multiphoton effects or strong correlations, none of which have been observed in extensive studies of $NbSe_2$. Extensive experiments on the BSTS material class have also never revealed any signatures of magnetic ordering or correlations. A more reasonable explanation could be offered by considering the effects of low critical currents, as observed previously in point-contact spectroscopic measurements.[41] It is possible that superconductivity induced into the topological surface states is rather weak, with critical currents as small as $I_c \simeq 1-3$ μA. Such a scenario would lead to a differential conductance dip when the current through the device exceeded the critical current, likely at a bias larger than the superconducting gap. However, this cannot explain the observation of multiple dips in our data. Additionally, such small critical currents are not consistent with disproportionately large magnetic fields ($B \simeq 2$ T) until which the ripples survive.

An interesting explanation for this effect is obtained by considering multiband Cooper pairing between different states residing on the TI surface. As shown schematically in Figure 4c, the topological surface states of a TI are usually accompanied by several closely spaced bands. Such bands may arise due to defect induced resonances,[42] bulk 2D subbands coexisting with the surface states at the chemical potential or band-bending induced spatial confinement of bulk states.[35,43] In the presence of induced superconducting order, multiple gaps may open up at finite energies away from the superconducting gap due to electron−hole mixing between the topological surface state and additional surface bands. To illustrate this effect we first evaluate the spectrum of Bogoliubov quasiparticles in a thin TI slab consisting of the topological surface state and a finite number of two-dimensional bulk bands, with the four possible types of

DOI: 10.1021/acsnano.8b07550
ACS Nano 2018, 12, 12665−12672

superconducting order $\Delta_{1,2,3,4}$ allowed by symmetry (see Supporting Information section E).

To aid clarity, we first choose theoretically convenient parameters, before describing a realistic simulation of a BSTS/$NbSe_2$ junction. In Figure 4d, we depict the spectral function $A(E,k)$ for an odd-parity Δ_2-type superconducting order, showing the Majorana Fermion *butterfly* spectrum at zero energy.[16,44] These in-gap states are the so-called surface Andreev bound states and essentially represent two-dimensional analogues of Majorana Fermions.[15−17,44,45] Accompanying this, we observe several finite-energy gaps corresponding to crossings of the topological surface states with the 2D bulk bands. The corresponding density of states is plotted in Figure 4e and shows several dips (marked by solid vertical lines) beyond the superconducting gap ($\Delta \simeq 0.1$ eV). Most spectacularly, it can be shown that the finite bias gaps appear only for those superconducting order symmetries that also lead to a Majorana Fermion mode at zero energy. This can be understood intuitively as a redistribution of spectral weight: level repulsion at higher energies pushes states into the gap, leading to the zero energy Majorana modes. Therefore, Majorana zero modes in such systems are always accompanied by mini-gaps at biases much larger than the primary superconducting gap. Additionally, the superconducting origin of the peak-dip features associated with these finite energy ripples may be gauged by evaluating their dependence on sample temperature. With increasing sample temperature, not only is the depth of the peak-dip structure reduced due to a reduction of the mini-gap amplitude, but also the voltage bias positions associated with these features are drawn closer to zero energy. This happens because the 2D sub-band levels, which were originally pushed away to larger energies by level repulsion due to the primary superconducting gap, are now drawn closer toward zero energy as the primary gap collapses. This is demonstrated by detailed simulations of the peak-dip structure of the ripples with decreasing values of superconducting gap amplitude provided in Supporting Information section F. This effect is exactly what is observed experimentally in Figure 2c,e, where the dip feature Δ_1 moves toward zero energy by $\simeq$1 meV, which matches very well with the primary superconducting gap amplitude $\Delta_0 \simeq 1.1$ meV due to $NbSe_2$.

Further, as shown in Figure 4e, at zero energy the density of states shows a large superconducting gap, and a small *dip* exactly at zero bias. This is despite the presence of a 2D Majorana mode and arises from the vanishing density of states of the linear spectrum of Majorana modes at zero energy.[45] This is of course contrary to the general belief that a Majorana mode must always lead to a conductance *peak* at zero bias. This is true only in one dimension; in higher dimensions, the zero mode generically leads to a conductance dip and is therefore difficult to separate from conductance dips arising from nontopological effects.[44,45] In such a scenario, the detection of superconducting conductance dips at large biases may offers an alternate test for topological superconductivity.

We now perform a realistic simulation of a heterojunction between $NbSe_2$ and BSTS and evaluate the spectrum of surface superconducting states. The work function of $NbSe_2$ is $\phi_{SC} \simeq$ 5.6−5.9 eV,[46,47] whereas that for BSTS is $\phi_{TI} \simeq$ 5.0−5.1 eV.[48] The large work function mismatch $\phi_{SC}-\phi_{TI} \simeq$ 0.5−0.9 eV between the two materials leads to p-type doping of BSTS and forces the chemical potential of the BSTS layer to get pinned at the valence band maxima. To perform a realistic band-structure calculation for BSTS, we tune the model parameters to fit the experimentally measured angle resolved photoemission spectrum of BSTS obtained from our previous work (see Supporting Information section H). In Figure 5a, we depict

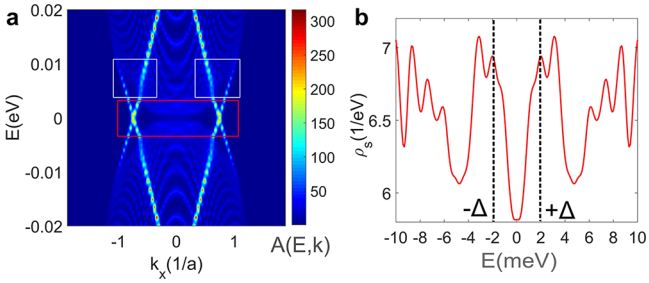

Figure 5. (a) Surface spectral function evaluated for a realistic interface between $NbSe_2$ and a 50 QL thick slab of BSTS. The red box depicts the 2D Majorana-type surface Andreev bound state. The white boxes depict the avoided crossings between the topological surface state and bulk-derived 2D sub-bands. (e) Corresponding density of states showing oscillations arising as a consequence of topological superconductivity.

the surface spectral function of a $N_z = 50$ QL thick BSTS slab with an induced superconducting gap $\Delta = 2.0$ meV. At zero energy, the *butterfly* spectrum arising from 2D surface Majorana Fermions is clearly observed (red box in Figure 5a). Simultaneously, the avoided crossing between the topological surface state band and the bulk-derived 2D sub-bands (marked using white boxes in Figure 5a) give rise to oscillations in the corresponding density of states, as shown in Figure 5b, at biases that are significantly larger than the induced superconducting gap. The ripples observed in our calculations are separated by $\simeq$2−3 meV in energy, exactly as observed in our experimentally measured differential conductance spectrum. Similar calculations are performed for BSTS slabs with thicknesses of $N_z = 20$ QL and $N_z = 35$ QL to obtain qualitatively similar results, but with larger energy scales separating the supergap dI−dV ripples (see Supporting Information section H). Qualitatively, the energy separation of the ripples can be estimated from the energy spacing between bulk-derived 2D sub-bands. In our experiments, the bulk bands originate from $J = 1/2$ Se(Te) p-type atomic orbitals, which form the valence band of our system with an experimentally measured bandwidth of $\Delta_{VB} \simeq 200$ meV[49] (see Supporting Information section G). This results in a sub-band spacing $\Delta_{SB} = \Delta_{VB}/N_z \simeq 4$ meV for a 50 QL layer slab. This simple estimation is in close agreement with the energy scale of 2−3 meV derived from the Green's function based density of states calculations. The appearance of differential conductance ripples at large biases in our experiments is therefore consistent with topological superconductivity in our samples. Similar ripples observed in a recent experiment on $Bi_2Se_3/NbSe_2$[25] junctions may also share a similar origin.

While the appearance of supergap ripples in the dI−dV spectrum strongly indicates the onset of topological superconductivity, the lack of a simple analytical expression to derive the positions of the ripples makes a direct comparison with experiments difficult. To enable such a comparison, band-structure calculations to identify the locations of the topological bands with respect to the trivial sub-bands will be required. Nonetheless, the mixing of the topological surface states with bulk-derived bands is *always* accompanied by the appearance of a 2D Majorana mode at zero energy making this

DOI: 10.1021/acsnano.8b07550
ACS Nano 2018, 12, 12665−12672

a rather generic feature of topological superconductivity. Combined with its rather striking experimental signature, namely, the appearance of superconducting ripples at biases much larger than the superconducting gap voltage, this method will serve as a litmus test for topological superconductivity for future researchers.

CONCLUSIONS

In all, we have provided three distinct arguments in favor of an observation of topological superconductivity in our samples: (i) the appearance of a two-gap spectrum, the larger gap associated with $NbSe_2$ and the smaller arising from a proximity induced gap of the topological surface states; (ii) an intrinsic asymmetry in the conductance spectrum that arises due to the linear density of states of the topological surface state dispersion and vanishes at temperatures and magnetic fields that destroy the proximity effect; (iii) differential conductance rippples at biases larger than the superconducting gap voltage that are explained as a consequence of multiband electron−hole mixing when topologically nontrivial superconducting order is induced. We propose that such features in differential conductance spectra can provide unambiguous tests for topological superconductivity. Our work therefore establishes the possibility of inducing superconductivity into the topological surface states of a bulk-insulating topological insulator. This work demonstrates the possibility of realizing p-wave superconductivity at topological insulator/superconductor interfaces as originally envisaged by Fu and Kane.[6]

METHODS

$BiSbTe_{1.25}Se_{1.75}$ single crystals are prepared using the modified Bridgman method. $NbSe_2$single crystals are prepared using the chemical vapor transport method. Thin flakes of $BiSbTe_{1.25}Se_{1.75}$ and $NbSe_2$ are exfoliated using the Scotch tape method. Heterostructures of $NbSe_2$/BSTS are prepared using the all-dry van der Waals transfer technique. E-beam lithography followed by e-beam evaporation of Cr/Au 10 nm/100 nm is used to define electrical contacts to the sample. Further details of device fabrication and single-crystal characterization can be found in Supporting Information sections A and B. Electrical transport experiments are performed using a low-frequency AC lock in method. The 10−20 nA of AC bias currents are used throughout the experiments. For differential conductance measurements, the DC bias is generated using a 16-bit digital-to-analog converter and is added to the AC bias within a home-built adder setup. All measurements reported here use a current biased scheme.

ASSOCIATED CONTENT

Supporting Information

The Supporting Information is available free of charge on the ACS Publications website at DOI: 10.1021/acsnano.8b07550.

Details of sample fabrication and characterization, Blonder−Tinkham−Klapwijk fitting of differential conductance data, theoretical modeling of topological insulator/superconductor interfaces, and raw differential conductance data (PDF)

AUTHOR INFORMATION

Corresponding Author

*E-mail: anil@iisc.ac.in.

ORCID

P. S. Anil Kumar: 0000-0002-4574-0868

Notes

The authors declare no competing financial interest.

ACKNOWLEDGMENTS

The authors thank Diptiman Sen and Jainendra K. Jain for helpful and insightful discussions. A.B. thanks MHRD, Govt. of India, for support. A.S. thanks KVPY, Govt. of India, for support. P.S.A.K. thanks Nanomission, Department of Science and Technology, Govt. of India, for support. The authors thank NNFC and MNCF, Centre for Nano Science and Engineering at the Indian Institute of Science Bangalore, for fabrication and characterization facilities.

REFERENCES

(1) Hasan, M. Z.; Kane, C. L. Colloquium: Topological Insulators. *Rev. Mod. Phys.* **2010**, *82*, 3045−3067.
(2) Qi, X.-L.; Zhang, S.-C. Topological Insulators and Superconductors. *Rev. Mod. Phys.* **2011**, *83*, 1057−1110.
(3) Chen, Y.; Analytis, J.; Chu, J.-H.; Liu, Z.; Mo, S.-K.; Qi, X.-L.; Zhang, H.; Lu, D.; Dai, X.; Fang, Z.; Zhang, S. C.; Fisher, I. R.; Hussain, Z.; Shen, Z.-X. Experimental Realization of a Three-Dimensional Topological Insulator, Bi_2Te_3. *Science* **2009**, *325*, 178−181.
(4) Xia, Y.; Qian, D.; Hsieh, D.; Wray, L.; Pal, A.; Lin, H.; Bansil, A.; Grauer, D.; Hor, Y. S.; Cava, R. J.; Hasan, M. Z. Observation of a Large Gap Topological Insulator Class With a Single Dirac Cone on the Surface. *Nat. Phys.* **2009**, *5*, 398−402.
(5) Hsieh, D.; Xia, Y.; Qian, D.; Wray, L.; Dil, J. H.; Meier, F.; Osterwalder, J.; Patthey, L.; Checkelsky, J. G.; Ong, N. P.; Fedorov, A. V.; Lin, H.; Bansil, A.; Grauer, D.; Hor, Y. S.; Cava, R. J.; Hasan, M. Z. A Tunable Topological Insulator in the Spin Helical Dirac Transport Regime. *Nature* **2009**, *460*, 1101−1105.
(6) Fu, L.; Kane, C. L. Superconducting Proximity Effect and Majorana Fermions at the Surface of a Topological Insulator. *Phys. Rev. Lett.* **2008**, *100*, 096407.
(7) Fu, L.; Kane, C. L. Probing Neutral Majorana Fermion Edge Modes with Charge Transport. *Phys. Rev. Lett.* **2009**, *102*, 216403.
(8) Potter, A. C.; Fu, L. Anomalous Supercurrent from Majorana States in Topological Insulator Josephson Junctions. *Phys. Rev. B: Condens. Matter Mater. Phys.* **2013**, *88*, 121109.
(9) Volovik, G. Fermion Zero Modes on Vortices in Chiral Superconductors. *JETP Lett.* **1999**, *70*, 609−614.
(10) Senthil, T.; Fisher, M. P. Quasiparticle Localization in Superconductors with Spin-Orbit Scattering. *Phys. Rev. B: Condens. Matter Mater. Phys.* **2000**, *61*, 9690−9698.
(11) Read, N.; Green, D. Paired States of Fermions in Two Dimensions with Breaking of Parity and Time-Reversal Symmetries and the Fractional Quantum Hall Effect. *Phys. Rev. B: Condens. Matter Mater. Phys.* **2000**, *61*, 10267−10297.
(12) Kitaev, A. Y. Unpaired Majorana Fermions in Quantum Wires. *Physics-Uspekhi* **2001**, *44*, 131−136.
(13) Hor, Y. S.; Williams, A. J.; Checkelsky, J. G.; Roushan, P.; Seo, J.; Xu, Q.; Zandbergen, H. W.; Yazdani, A.; Ong, N. P.; Cava, R. J. Superconductivity in $Cu_xBi_2Se_3$ and its Implications for Pairing in the Undoped Topological Insulator. *Phys. Rev. Lett.* **2010**, *104*, 057001.
(14) Sasaki, S.; Kriener, M.; Segawa, K.; Yada, K.; Tanaka, Y.; Sato, M.; Ando, Y. Topological Superconductivity in $Cu_xBi_2Se_3$. *Phys. Rev. Lett.* **2011**, *107*, 217001.
(15) Fu, L.; Berg, E. Odd-Parity Topological Superconductors: Theory and Application to $Cu_xBi_2Se_3$. *Phys. Rev. Lett.* **2010**, *105*, 097001.
(16) Hao, L.; Lee, T. Surface Spectral Function in the Superconducting State of a Topological Insulator. *Phys. Rev. B: Condens. Matter Mater. Phys.* **2011**, *83*, 134516.
(17) Nakosai, S.; Tanaka, Y.; Nagaosa, N. Topological Superconductivity in Bilayer Rashba System. *Phys. Rev. Lett.* **2012**, *108*, 147003.

DOI: 10.1021/acsnano.8b07550
ACS Nano 2018, 12, 12665−12672

(18) Sasaki, S.; Ren, Z.; Taskin, A.; Segawa, K.; Fu, L.; Ando, Y. Odd-Parity Pairing and Topological Superconductivity in a Strongly Spin-Orbit Coupled Semiconductor. *Phys. Rev. Lett.* **2012**, *109*, 217004.
(19) Zhang, D.; Wang, J.; DaSilva, A. M.; Lee, J. S.; Gutierrez, H. R.; Chan, M. H. W.; Jain, J.; Samarth, N. Superconducting Proximity Effect and Possible Evidence for Pearl Vortices in a Candidate Topological Insulator. *Phys. Rev. B: Condens. Matter Mater. Phys.* **2011**, *84*, 165120.
(20) Williams, J. R.; Bestwick, A. J.; Gallagher, P.; Hong, S. S.; Cui, Y.; Bleich, A. S.; Analytis, J. G.; Fisher, I. R.; Goldhaber-Gordon, D. Unconventional Josephson Effect in Hybrid Superconductor-Topological Insulator Devices. *Phys. Rev. Lett.* **2012**, *109*, 056803.
(21) Veldhorst, M.; Snelder, M.; Hoek, M.; Gang, T.; Guduru, V.; Wang, X.; Zeitler, U.; van der Wiel, W. G.; Golubov, A.; Hilgenkamp, H.; Brinkman, A. Josephson Supercurrent through a Topological Insulator Surface State. *Nat. Mater.* **2012**, *11*, 417−421.
(22) Liu, H.-C.; He, H.-T.; Li, B.-K.; Liu, S.-G.; Lin He, Q.; Wang, G.; Sou, I.-K.; Wang, J. Interface effect in Nb-Bi_2Te_3 Hybrid Structure. *Appl. Phys. Lett.* **2013**, *103*, 152601.
(23) Zareapour, P.; Hayat, A.; Zhao, S. Y. F.; Kreshchuk, M.; Jain, A.; Kwok, D. C.; Lee, N.; Cheong, S.-W.; Xu, Z.; Yang, A.; Gu, G. D.; Jia, S.; Cava, R. J.; Burch, K. S. Proximity-Induced High-Temperature Superconductivity in the Topological Insulators Bi_2Se_3 and Bi_2Te_3. *Nat. Commun.* **2012**, *3*, 1056.
(24) Yang, F.; Ding, Y.; Qu, F.; Shen, J.; Chen, J.; Wei, Z.; Ji, Z.; Liu, G.; Fan, J.; Yang, C.; Xiang, T.; Lu, L. Proximity Effect at Superconducting Sn-Bi_2Se_3 Interface. *Phys. Rev. B: Condens. Matter Mater. Phys.* **2012**, *85*, 104508.
(25) Li, H.; Zhou, T.; He, J.; Wang, H.-W.; Zhang, H.; Liu, H.-C.; Yi, Y.; Wu, C.; Law, K. T.; He, H.; Wang, J. Origin of Bias-Independent Conductance Plateaus and Zero-Bias Conductance Peaks in $Bi_2Se_3/NbSe_2$ Hybrid Structures. *Phys. Rev. B: Condens. Matter Mater. Phys.* **2017**, *96*, 075107.
(26) Dai, W.; Richardella, A.; Du, R.; Zhao, W.; Liu, X.; Liu, C.; Huang, S.-H.; Sankar, R.; Chou, F.; Samarth, N.; Li, Q. Proximity-Effect-Induced Superconducting Gap in Topological Surface States−A Point Contact Spectroscopy Study of $NbSe_2/Bi_2$ Se_3 Superconductor-Topological Insulator Heterostructures. *Sci. Rep.* **2017**, *7*, 7631.
(27) Xu, J.-P.; Wang, M.-X.; Liu, Z. L.; Ge, J.-F.; Yang, X.; Liu, C.; Xu, Z. A.; Guan, D.; Gao, C. L.; Qian, D.; Liu, Y.; Wang, Q. H.; Zhang, F. C.; Xue, Q. K.; Jia, J. F. Experimental Detection of a Majorana Mode in the Core of a Magnetic Vortex inside a Topological Insulator-Superconductor Bi_2 $Te_3/NbSe_2$ Heterostructure. *Phys. Rev. Lett.* **2015**, *114*, 017001.
(28) Sun, H.-H.; Zhang, K.-W.; Hu, L.-H.; Li, C.; Wang, G.-Y.; Ma, H.-Y.; Xu, Z.-A.; Gao, C.-L.; Guan, D.-D.; Li, Y.-Y.; Liu, C.; Qian, D.; Zhou, Y.; Fu, L.; Li, S. C.; Zhang, F. C.; Jia, J. F. Majorana Zero Mode Detected with Spin Selective Andreev Reflection in the Vortex of a Topological Superconductor. *Phys. Rev. Lett.* **2016**, *116*, 257003.
(29) He, Q. L.; Pan, L.; Stern, A. L.; Burks, E. C.; Che, X.; Yin, G.; Wang, J.; Lian, B.; Zhou, Q.; Choi, E. S.; Murata, K.; Kou, X.; Chen, Z.; Nie, T.; Shao, Q.; Fan, Y.; Zhang, S. C.; Liu, K.; Xia, J.; Wang, K. L. Chiral Majorana Fermion Modes in a Quantum Anomalous Hall Insulator−Superconductor Structure. *Science* **2017**, *357*, 294−299.
(30) Chang, C.-Z.; Zhang, J.; Feng, X.; Shen, J.; Zhang, Z.; Guo, M.; Li, K.; Ou, Y.; Wei, P.; Wang, L.-L.; Ji, Z. Q.; Feng, Y.; Ji, S.; Chen, X.; Jia, J.; Dai, X.; Fang, Z.; Zhang, S. C.; He, K.; Wang, Y.; et al. Experimental Observation of the Quantum Anomalous Hall Effect in a Magnetic Topological Insulator. *Science* **2013**, *340*, 167−170.
(31) Mogi, M.; Kawamura, M.; Yoshimi, R.; Tsukazaki, A.; Kozuka, Y.; Shirakawa, N.; Takahashi, K.; Kawasaki, M.; Tokura, Y. A Magnetic Heterostructure of Topological Insulators as a Candidate for an Axion Insulator. *Nat. Mater.* **2017**, *16*, 516−521.
(32) Xu, Y.; Miotkowski, I.; Chen, Y. P. Quantum Transport of Two Species Dirac Fermions in Dual-gated Three-dimensional Topological Insulators. *Nat. Commun.* **2016**, *7*, 11434.
(33) Stehno, M. P.; Hendrickx, N. W.; Snelder, M.; Scholten, T.; Huang, Y.; Golden, M. S.; Brinkman, A. Conduction Spectroscopy of a Proximity Induced Superconducting Topological Insulator. *Semicond. Sci. Technol.* **2017**, *32*, 094001.
(34) Tikhonov, E.; Shovkun, D.; Snelder, M.; Stehno, M.; Huang, Y.; Golden, M.; Golubov, A. A.; Brinkman, A.; Khrapai, V. Andreev Reflection in an s-Type Superconductor Proximized 3D Topological Insulator. *Phys. Rev. Lett.* **2016**, *117*, 147001.
(35) Banerjee, A.; Sundaresh, A.; Majhi, K.; Ganesan, R.; Anil Kumar, P. S. Accessing Rashba States in Electrostatically Gated Topological Insulator Devices. *Appl. Phys. Lett.* **2016**, *109*, 232408.
(36) Banerjee, A.; Sundaresh, A.; Biswas, S.; Ganesan, R.; Sen, D.; Anil Kumar, P. S. Quantized Transport in Topological Insulator npn Junctions. *arXiv: 1803.11367* **2018**.
(37) Blonder, G.; Tinkham, M.; Klapwijk, T. Transition from Metallic to Tunneling Regimes in Superconducting Microconstrictions: Excess Current, Charge Imbalance, and Supercurrent Conversion. *Phys. Rev. B: Condens. Matter Mater. Phys.* **1982**, *25*, 4515−4532.
(38) Rowell, J.; Chynoweth, A.; Phillips, J. Multiphonon Effects in Tunnelling Between Metals and Superconductors. *Phys. Rev. Lett.* **1962**, *9*, 59−61.
(39) Jourdan, M.; Huth, M.; Adrian, H. Superconductivity Mediated by Spin Fluctuations in the Heavy-Fermion Compound UPd_2Al_3. *Nature* **1999**, *398*, 47−49.
(40) Xi, X.; Wang, Z.; Zhao, W.; Park, J.-H.; Law, K. T.; Berger, H.; Forró, L.; Shan, J.; Mak, K. F. Ising Pairing in Superconducting $NbSe_2$ Atomic Layers. *Nat. Phys.* **2016**, *12*, 139−143.
(41) Sheet, G.; Mukhopadhyay, S.; Raychaudhuri, P. Role of Critical Current on the Point-Contact Andreev Reflection Spectra between a Normal Metal and a Superconductor. *Phys. Rev. B: Condens. Matter Mater. Phys.* **2004**, *69*, 134507.
(42) Xu, Y.; Chiu, J.; Miao, L.; He, H.; Alpichshev, Z.; Kapitulnik, A.; Biswas, R. R.; Wray, L. A. Disorder Enabled Band Structure Engineering of a Topological Insulator Surface. *Nat. Commun.* **2017**, *8*, 14081.
(43) Lee, J.; Park, J.; Lee, J.-H.; Kim, J. S.; Lee, H.-J. Gate-tuned Differentiation of Surface-Conducting States in $Bi_{1.5}Sb_{0.5}Te_{1.7}Se_{1.3}$ Topological-Insulator Thin Crystals. *Phys. Rev. B: Condens. Matter Mater. Phys.* **2012**, *86*, 245321.
(44) Hsieh, T. H.; Fu, L. Majorana Fermions and Exotic Surface Andreev Bound States in Topological Superconductors: Application to $Cu_xBi_2Se_3$. *Phys. Rev. Lett.* **2012**, *108*, 107005.
(45) Sato, M.; Ando, Y. Topological Superconductors: A Review. *Rep. Prog. Phys.* **2017**, *80*, 076501.
(46) Liu, Y.; Stradins, P.; Wei, S.-H. Van der Waals Metal-Semiconductor Junction: Weak Fermi Level Pinning Enables Effective Tuning of Schottky Barrier. *Sci. Adv.* **2016**, *2*, No. e1600069.
(47) Shimada, T.; Ohuchi, F. S.; Parkinson, B. A. Work Function and Photothreshold of Layered Metal Dichalcogenides. *Jpn. J. Appl. Phys.* **1994**, *33*, 2696−2698.
(48) Takane, D.; Souma, S.; Sato, T.; Takahashi, T.; Segawa, K.; Ando, Y. Work Function of Bulk-Insulating Topological Insulator $Bi_{2-x}Sb_xTe_{3-y}Se_y$. *Appl. Phys. Lett.* **2016**, *109*, 091601.
(49) Lohani, H.; Mishra, P.; Banerjee, A.; Majhi, K.; Ganesan, R.; Manju, U.; Topwal, D.; Kumar, P. S. A.; Sekhar, B. Band Structure of Topological Insulator $BiSbTe_{1.25}Se_{1.75}$. *Sci. Rep.* **2017**, *7*, 4567.

DOI: 10.1021/acsnano.8b07550
ACS Nano 2018, 12, 12665−12672